

TRANSFER TO MULTI-CIRCLE ELLIPTIC HALO ORBIT IN EARTH-MOON ELLIPTIC RESTRICTED THREE-BODY PROBLEM

Hao PENG⁽¹⁾, and Shijie XU⁽²⁾

⁽¹⁾⁽²⁾*School of Astronautics, Beihang University, Beijing, China, AstroH.Peng@gmail.com*

Abstract: *The Multi-circle Elliptic Halo (ME-Halo) orbit is a special kind of symmetric periodic orbits generated in Elliptic Restricted Three-Body Problem (ERTBP). Its special properties, including long period and redundant stable manifold, make it a promising nominal orbit in space mission design. In this paper the direct transfer to lunar ME-Halo orbits with two impulsive maneuvers is investigated. At first perigee transfers are constructed, then different orbit injection points are surveyed and the manifold injection point is optimized. At last the redundant stable manifold of the ME-Halo orbit is demonstrated to have great impact on the transfer trajectory design. Results in this paper enriches the preliminary space mission design options by providing feasible strategies to reach ME-Halo orbits in Earth-Moon system.*

Keyword: *ERTBP, ME-Halo, Direct transfer, Stable manifolds, Space mission design.*

1. Introduction

Since Euler first found three collinear libration points of Circular Restricted Three-Body Problem (CRTBP) in 1767 and Lagrange found the other two triangular libration points in 1772 [1], many mysteries in this fascinating field have been revealed and fruitful applications in space exploration have been yielded. In 1967 Szebehely comprehensively surveyed both analytical and numerical outcomes until his time [2]. Then spatial halo orbit was discovered [3] and constructed analytically [4] and numerically [5]. Modern methods including WSB theory [6] and dynamical system theory [7–9]. Recently Parker and Anderson gave a comprehensive summary of the lunar transfer trajectory design in their book, which covers the transfer to all kinds of libration orbits and low lunar orbits by both direct and low-energy transfer under CRTBP, patched CRTBP and JPL ephemeris models [10]. Most results in the book is developed in CRTBP and they claimed that the most notable influence is the lunar eccentricity.

The motion of planets in the solar system is better described by Keplerian orbits with eccentricity e ranging from 0.0086 to 0.2488 [11]. Results in CRTBP are extended to the Elliptic Restricted Three-Body Problem (ERTBP) model. Moulton stated the strong periodicity criteria of symmetric periodic orbits in planar ERTBP [12] and Broucke constructed libration periodic orbits under this criteria and investigated their stability systematically [13]. Sarris then extended this study to spatial ERTBP and divided the stability region analytically [14]. But the periodic orbit they studied is less likely to be useful in practical mission design. Recently Hou and Liu constructed series expansion of collinear libration point orbits in ERTBP by Lindstedt-Poincare method [15]. The result is lengthy and complex because the appearance of eccentricity greatly increases the number of terms. Mission design under ERTBP draws attentions as well. Campagnola et al. designed the Mercury capture stage of the BepiColombo mission in ERTBP model by ergodic search and then he found the resulted ballistic capture shadowed the manifold of a halo like orbit around the libration region of the Sun-Mercury ERTBP [16]. Qi and Xu applied Lagrange coherent structure method to construct lunar transfer trajectory shadowing the

time-dependent manifold in ERTBP model [17, 18]. Their study gives a clear view of the effect of eccentricity e on the transfer trajectory and handle other perturbations but the computation cost a lot of time. Recently Qi, Xu and et al. had studied the ballistic capture in mercury ERTBP and their results focus on the near Earth launch conditions [19]. Peng and Xu systematically investigated the stability of Multi-circle Elliptic Halo (ME-Halo) orbits in ERTBP [20], which was complex and greatly different from halo orbits in CRTBP.

In this paper ME-Halo orbits are derived and numerically generated first, with a review of that ME-Halo orbits can possess two stable manifold direction. The author constructs direct transfer to lunar ME-Halo orbits with two impulsive transfer in ERTBP. The energy cost is analyzed by the velocity cost during the transfer. Then the manifold injection point is optimized within a bounded interval and optimal transfers are found to occur around apogees of stable manifolds. At last the impact of the redundant stable manifold of ME-Halo is discussed. The result in this paper demonstrated the feasibility of arriving ME-Halo and provides new options for future mission design.

2. Backgrounds

2.1. ERTBP and CRTBP

The full three body problem has no complete solution because there are 18 first order differential equations but only 10 general integrals. An intuitive approach is to study the restricted three body problem (RTBP), where the mass of one body tends to zero and does not affect primaries' motion. In RTBP the motion of the infinitesimal third body under the attraction of two primaries' gravity fields is of interests. In this section a brief review of the equation of motion for the spacecraft in the ERTBP and the CRTBP model is given.

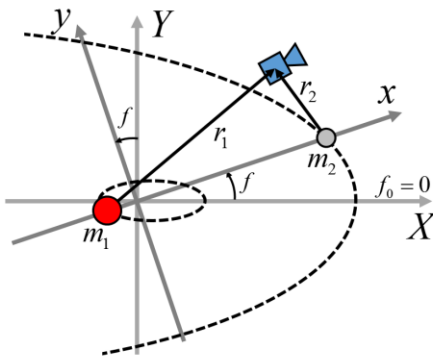


Figure 1. Barycenter Inertial coordinate frame (X, Y, Z) and Barycenter Synodic coordinate frame (x, y, z) . The z -axis finishes the right handed system by pointing out of the paper. In ERTBP the primary orbit (dashed arc) is elliptical while in CRTBP it is circular.

In ERTBP primaries rotate each other on a Keplerian elliptic orbits with eccentricity e around their common barycenter (dashed ellipse in Fig. 1). The distance between primaries r_{12} is changing with true anomaly f thus with time t , and is given by

$$r_{12}(f) = \frac{a_{12}(1-e^2)}{1+e \cos f}$$

where a_{12} is the semimajor axis of primaries. The synodic pulsating coordinate frame is introduced as illustrated in Fig. 1. The origin locates at the primary barycenter. The x -axis points from the larger primary m_1 to the smaller one m_2 . The z -axis is parallel with the angular momentum (pointing out of the paper) and the y -axis finishes the right-handed system. The system is instantaneously scaled by the primary distance $r_{12}(f)$, the total primary mass $(m_1 + m_2)$ and the reciprocal of the mean angular velocity \bar{n} . In this frame primaries are fixed at $x_1 = -\mu$ and $x_2 = 1 - \mu$ and the frame is pulsating. Furthermore, the independent variable of the system is transformed from time t to true anomaly f by the chain rule

$$\frac{d}{dt} = \frac{df}{dt} \frac{d}{df}$$

Where

$$\frac{df}{dt} = \frac{G(m_1 + m_2)^{1/2}}{a^{3/2}(1-e^2)^{3/2}} (1+e \cos f)^2 \quad (1)$$

In this way, equations of motion of the third body in ERTBP is given by [2]

$$\begin{aligned} x'' - 2y' &= \omega_x \\ y'' + 2x' &= \omega_y \\ z'' &= \omega_z \end{aligned} \quad (2)$$

where

$$\omega(x, y, z, f) = (1+e \cos f)^{-1} \tilde{\Omega}(x, y, z) \quad (3)$$

$$\tilde{\Omega}(x, y, z) = \Omega(x, y, z) - \frac{1}{2} e \cos f z^2 \quad (4)$$

$$\Omega(x, y, z) = \frac{1}{2}(x^2 + y^2) + \frac{1-\mu}{r_1} + \frac{\mu}{r_2} + \frac{1}{2} \mu(1-\mu) \quad (5)$$

with $r_1 = \sqrt{(x+\mu)^2 + y^2 + z^2}$ and $r_2 = \sqrt{(x-1+\mu)^2 + y^2 + z^2}$. Primes over x , y and z indicate the differential respect to true anomaly f . The epoch when primaries are at their periapsis is set to be $f_0 = 0$ as illustrated in Fig. 1. It is worth noting that ERTBP implicitly depends on time t through Eq. 1. And because of the trigonometric function introduced by Eqs. 1, 3 and 4, ERTBP

is a non-autonomous system with period 2π . There is no Jacobi constant in the system anymore. Multiplied Eq. 2 by \dot{x} , \dot{y} and \dot{z} respectively, add them up and integrate, we have

$$\dot{x}^2 + \dot{y}^2 + \dot{z}^2 = 2 \int (\omega_x dx + \omega_y dy + \omega_z dz) \quad (6)$$

Since ω depends also on the true anomaly f , the expression under the integral is not a total differential. Instead we have

$$d\omega = (\omega_x dx + \omega_y dy + \omega_z dz) + \omega_f df$$

Substitute it into Eq. 6 and we have

$$\dot{x}^2 + \dot{y}^2 + \dot{z}^2 = 2\omega - 2 \int_{f_0}^f \omega_f d\tau - C(f_0) \quad (7)$$

The term 2ω is the amended potential of the third body in synodic frame. The integral term is caused by the pulsating of the system. The integral constant $C(f_0)$ depends on the initial anomaly f now. For the CRTBP model where the eccentricity e is zero, equations of motion is obtained by substitute $e=0$ into the ERTBP model. Then Eqs. 3, 4 and 5 degenerate to one equation, and the integral term in Eq. 7 vanishes and $C(f_0)$ degenerates to the traditional Jacobi integral C in CRTBP.

2.2. ME-Halo Orbits

In CRTBP, the halo orbit is numerically constructed from the third order analytical approximation by differentially correction method. Because of terms with e in the equation of motion in ERTBP, circular halo orbits are not strictly periodic anymore, though they can be close up by differential correction for certain duration. Campagnola stated the periodicity criteria that symmetric periodic orbits in ERTBP must perpendicularly cross the x - z plane twice when primaries are at their apsis [16]. Therefore periodic orbits in CRTBP surviving from the eccentricity perturbation must obtain a commensurable period with the primary system. Then they can be continued into ERTBP by gradually increasing the eccentricity e . The planar and vertical Lyapunov orbit with large amplification have period large enough to be integral multiple of the primary period 2π [13, 14], but halo orbits usually have period less than $3/4\pi$. So only halo orbits with rational multiples of 2π is possible. The measurable constrain can be expressed as

$$T_C = T_E / M = 2N / M\pi, \quad M, N \in \mathbb{R}^+$$

where T_C is the circular halo orbit period and T_E is the period of the continued periodic orbit in ERTBP. They are referred to as *Multi-circle Elliptic Halo (ME-Halo)* orbits hereinafter since the emphasis is paid on their multi-circle property. For clarity halo orbits in CRTBP are referred to as *circular halo orbits*. ME-Halo orbits can be classified into four groups according to their

starting states and they have different stability properties [20]:

- **Periapsis Group:** Odd M ; Primaries at Periapsis; Start from left side of orbit.
- **Apoapsis Group:** Odd M ; Primaries at Apoapsis; Start from left side of orbit.
- **Left Group:** Even M ; Primaries at Periapsis; Start from left side of orbit.
- **Right Group:** Even M ; Primaries at Periapsis; Start from right side of orbit.

It is noteworthy that T_E is M times of T_C , so the integral time will be large. The traditional differential correction method can be failed by an inaccurate initial guess. Considering the method is essentially a Newton's method and borrowing the idea of multiple shooting method [5], the generation of ME-Halo can be rewritten into an multi-segment optimization problem [20], which is less insensitive to the initial guess and easier to program.

The stable direction of ME-Halo orbits is obtained through their monodromy matrix Ψ . It is obtained by integrate the transition matrix $\Phi(f, f_0)$ for a full period, which satisfies

$$\dot{\Phi}(f, f_0) = A_E(X, f)\Phi(f, f_0), \quad \Phi(f_0, f_0) = I_6$$

where $A_E(X, f)$ is the Jacobian of the equation 2

$$A_E(X, f) = \begin{bmatrix} 0 & I_3 \\ H_E & K_E \end{bmatrix}_{(X, f)}, \quad H_E = \begin{bmatrix} \omega_{xx} & \omega_{xy} & \omega_{xz} \\ \omega_{yx} & \omega_{yy} & \omega_{yz} \\ \omega_{zx} & \omega_{zy} & \omega_{zz} \end{bmatrix}_{(X, f)}, \quad K_E = \begin{bmatrix} 0 & 2 & 0 \\ -2 & 0 & 0 \\ 0 & 0 & 0 \end{bmatrix}.$$

Six eigenvalues of Ψ come in reciprocal pairs as

$$\lambda_1, 1/\lambda_1, \lambda_2, 1/\lambda_2, \lambda_3, 1/\lambda_3$$

In CRTBP circular halos have $\lambda_1 = 1$, real $\lambda_2 > 1$ and complex unit λ_3 , but in ERTPB the situation is much more complex and ME-Halo orbits can have two pairs of real eigenvalues as discussed by Peng and Xu [20]. Each real eigenvalue smaller than one indicates a stable direction spanning the stable manifold asymptotically approaching the periodic orbit. So if the redundant direction exists, the ME-Halo orbit will span a three-dimensional manifold, which is different from the two-dimensional manifold of circular halo orbits. According to their study, Earth-Moon L_1 Perigee ME-Halo with $M5N2$ has two real pairs of eigenvalues.

2.3. Lunar ME-Halo Orbits and Parameterize

The target orbit of the transfer in this paper is the Earth-Moon L_1 Perigee ME-Halo with $M5N2$, as demonstrated in Fig. 2. The orbit is generated by choosing a set of (M, N) from the whole circular halo orbit family in CRTBP, gradually increasing the primary eccentricity e and adjusting the initial condition by the multi-segment optimization method [20]. Points on

ME-Halos are parameterized by $\tau \in [0,1)$ where $\tau=0$ is the starting point and $\tau=1$ is the returning point after one period which should close up the orbit. As shown in the right plot, the separation for each circle is not equal but roughly $\Delta\tau=0.2$.

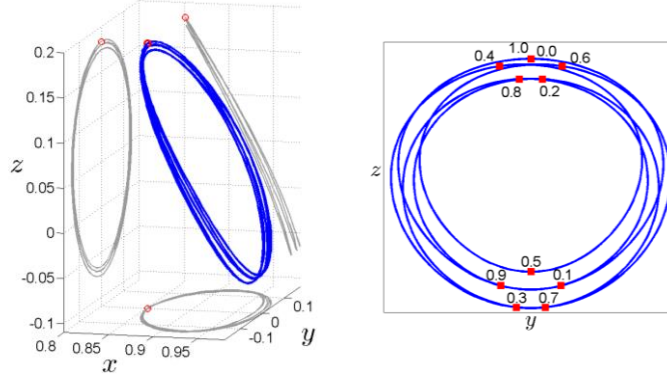


Figure 2. The Earth-Moon L_1 Periapsis ME-Halo orbit with $M5N2$ and the illustration of point parameterization by $\tau \in [0,1)$, where $\tau=0$ is the starting point and $\tau=1$ is the returning point after one period.

The stable direction of point τ is given by the characteristic eigenvector of the monodromy matrix $\Psi(\tau)$. Then a position perturbation of ϵ is applied along this direction, and the velocity perturbation is applied proportionally. The stable manifold is generated by backward integration. Attentions should be paid that according to the previous discussion the target orbit have two stable directions. Only the major direction with smallest eigenvalue will be considered in the following transfer trajectory design. The significant impact of the additional stable direction is discussed in section 4. The stable direction and its reverse can lead the spacecraft to opposite side of the ME-Halo. To be consistent with Parker and Anderson the direction leading to the Moon is referred to as *internal direction* and the one leading to the Earth as *external direction*. In Fig. 3, external and internal major stable manifolds with same perturbation and duration of the ME-Halo orbit are demonstrated. Cautions should be paid that the duration is measured by the independent variable f here.

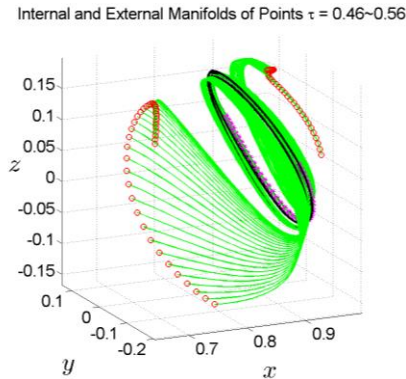


Figure 3. Internal and external manifolds associated points $\tau = 0.46 \sim 0.56$ on the lunar L_1 periapsis ME-Halo orbit with $M5N2$.

3. Direct Transfer with Two Impulsive Maneuvers

The period of ME-Halo orbits T_E is M times of the circular halo period T_C and N times of the primary period 2π , so once a spacecraft is accurately injected into a ME-Halo orbit it will drift for a long time. Even in real Earth-Moon system the ME-Halo orbit will diverge slower than circular halo orbits since it has taken the lunar eccentricity into consideration, which perturbs the motion of the spacecraft most [10]. Therefore it is of value to find out a way to arrive such an orbit. In this section the strategy to design a direct transfer to the ME-Halo orbit with two impulsive maneuvers in ERTBP is presented and the transfer is optimized as well.

3.1. Modeling the Transfer

The stable manifold of libration periodic orbits has been used as a fruitful approach to design direct low-energy transfer. In this paper the author follows similar ideas and processes Parker and Anderson used to investigate lunar libration point orbit transfer in CRTBP [10]. Since the non-autonomous ERTBP governs the motion, both periodic orbits and their manifolds are time-dependent now. This feature leads to that any transfer designed is attached to a specific Earth-Moon phase which cannot be delayed or preceded. For example if primaries are at the epoch f^* , the spacecraft can only be located at the point corresponding to $f^* + 2\pi \cdot n$ on ME-Halo or its manifolds.

The transfer trajectory is divided into two parts: first from the parking LEO to the stable manifold of target ME-Halo orbit, named *bridge segment* since it connects the two trajectories; second along the manifold to the ME-Halo named *manifold segment*. During the designing the trajectory is integrated backwardly. The strategy can be summarized as following:

Step 1. Construct the desired ME-Halo orbit.

- i. Generate the whole circular halo orbit family.
- ii. Choose an appropriated circular halo orbit with $T_C = 2N\pi / M$.
- iii. Continue the chosen orbit to the ME-Halo orbit with $T_E = 2N\pi$ in Earth-Moon ERTBP.

Step 2. Construct the manifold segment.

- i. Choose a target point τ on the ME-Halo orbit.
- ii. Set the transfer direction (internal or external), and generate the stable direction. Then apply a position perturbation ϵ along the chosen direction to obtain the *orbit injection (OI)* point $X_{OI} = X(\tau_\epsilon)$.
- iii. Backward integrate from the OI point until the *manifold injection (MI)* point X_{MI} .

Step 3. Construct the bridge segment.

- i. Define the manifold injection maneuver ΔV_{MI} to be tangent with V_{MI} .
- ii. Apply the maneuver and backward integrate until reach the LEO parking orbit with height r_{LEO} .

Step 4. Repeat process 3 and adjust ΔV_{MI} until a tangent arrival at the LEO obtained.

Step 5. Define the LEO departing maneuver ΔV_{LEO} to be tangent with the LEO. Calculate it.

The process of Step 4 is solved as an optimization problem here, whose initial guess is constructed by Hohmann transfer in two-body problem. For simplicity the LEO is chosen as a circular orbit. In this way a successful three-dimensional direct transfer from the parking LEO to the point τ on the given ME-Halo orbit in ERTBP model is constructed.

3.2. Perigee Transfer

An intuitive way is to choose the MI point X_{MI} as the first perigee near the Earth, where the velocity and position vectors should be orthogonal in Earth-centered Inertial coordinate frame. The pulsating of the ERTBP synodic frame should also be taken into consideration. Then following the strategy described above, exterior and interior transfer trajectory examples leading to different OI point τ on ME-Halo are constructed and demonstrated in Fig. 4 and Fig. 5 respectively. Parameters used in this paper can be found in Tab. 1. The external transfer trajectory approaches the ME-Halo orbit after ΔV_{MI} , while the internal transfer trajectory encounters a lunar flyby before the final approach. This indicates that an internal transfer can be more efficient if the lunar flyby is carefully chosen. However, companied lunar flybys make the trajectory very sensitive to initial conditions and some even escape through L_2 region after flyby, so only the exterior transfer trajectory is surveyed in the following study. The sharp turn at the maneuver point is a visual effect in synodic frame. It is worth noting that the manifold is measured by true anomaly interval, hence these illustrated manifolds do not guarantee same time duration but depending on df/dt .

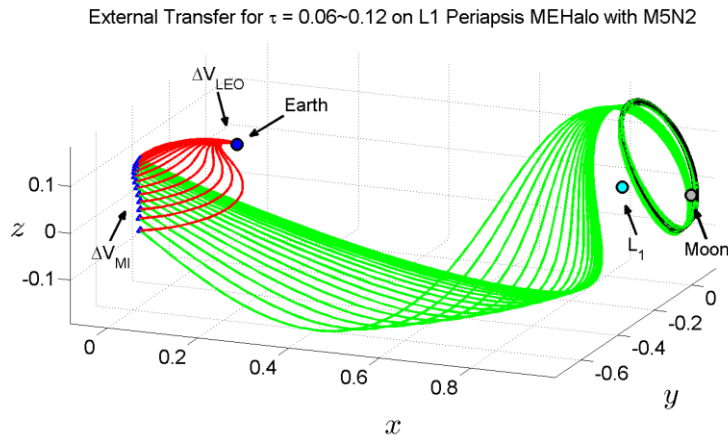


Figure 4. External transfer from the parking LEO to orbit injection points $\tau = 0.06 \sim 0.12$ on L_1 Perigee ME-Halo with $M5N2$.

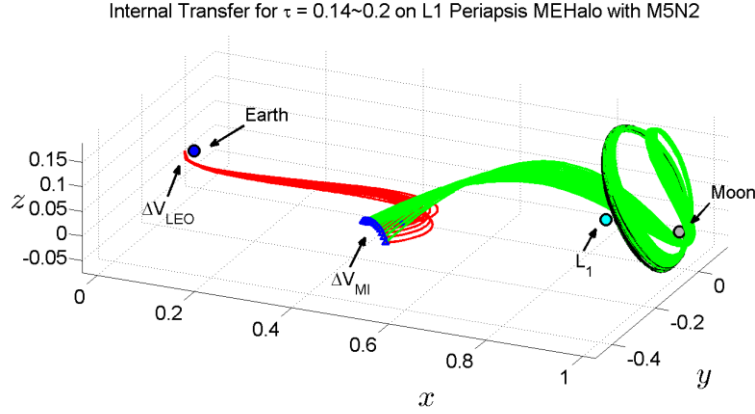


Figure 5. Internal transfer from the parking LEO to orbit injection points $\tau = 0.14 \sim 0.2$ on L_1 Periapsis ME-Halo with M5N2.

Table 1. Parameters and tolerance used to construct direct transfers in the paper.

Parameters	Value / Unit
Earth-Moon semimajor axis a	384400 km
Earth-Moon period	27.5 days
Earth-Moon mass ratio μ	0.0122
Earth-Moon eccentricity e	0.0554
Target orbit	L_1 ME-Halo with M5N2
Transfer direction	External
Position perturbation ϵ	100 m
Parking LEO height r_{LEO}	185 km
Max integrate interval Δf_{max}	6π
Integration tolerance	1×10^{-10}
Optimization tolerance	1×10^{-7}

Different target points τ on the same ME-Halo orbit are surveyed. 500 OI points along the orbit are chosen uniformly along the orbit and external transfers to these points are constructed. In Fig. 6 the resulted velocity cost is depicted with respect to the orbit injection point τ , where ΔV ranges from 3.791 km/s to 4.676 km/s. There is a five-interval periodicity corresponding to the multi-circles properties of ME-Halo. In each interval the curve is smooth but fluctuates slightly differently, which justifies that ME-Halo is not a simple repeat of circular halo orbits. Their connections are discontinuous. Transfers around the discontinue region (framed thin region) around $\tau = 0.3$ are illustrated in Fig. 7, which explains that this discontinuity is caused by the max distance restriction (0.7 normalized length) of the perigee during calculation. When the first manifold perigee locates too far, the program automatically jumps to the next perigee and the transfer is constructed there.

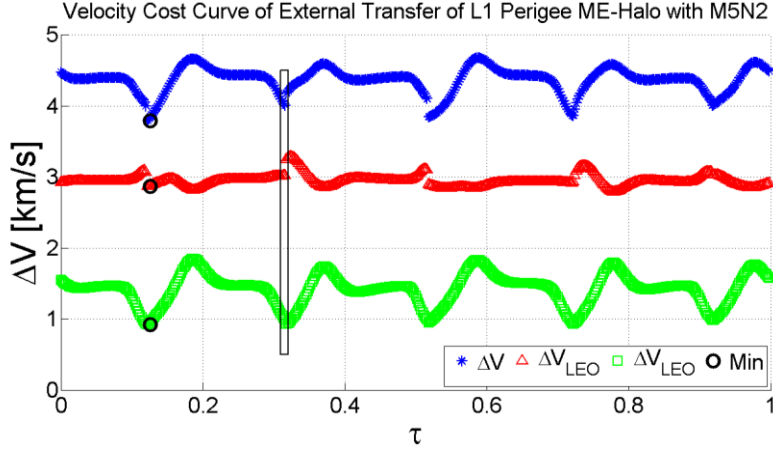


Figure 6. Velocity cost curves of external direct transfer to different orbit injection points on ME-Halo. Transfers in the framed thin region is demonstrated in next figure.

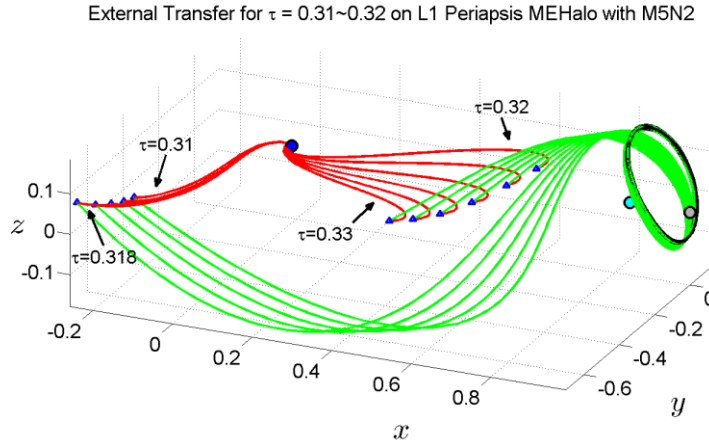


Figure 7. Transfer trajectories to points $\tau = 0.31 \sim 0.32$ around the discontinuous point (framed thin region in previous figure). The discontinuity is caused by the max distance restriction of the perigee.

3.3. Optimize the Manifold Injection Point

In the previous discussion orbit injection points with least velocity cost can be extracted from the survey on OI points. However it is not quite reasonable to choose the perigee as the MI point. Let the MI point parameterized by s , which is the true anomaly of the MI point counting from the OI point τ backwardly. Vary s and the transfers should be different. For example, vary the MI point s on the manifold associated with OI point $\tau = 0.22$, direct transfers are constructed as presented in Fig. 8 and the corresponding ΔV is presented in Fig. 9. It can be observed that all MI points can be reached and the velocity cost varies smoothly. The perigee transfer (marked by dashed vertical line) costs nearly the most ΔV and the optimal transfer occurs around $s = -12.5$ which is almost at the apogee. Also there tends to be other local optimal MI points if let s stretch broader.

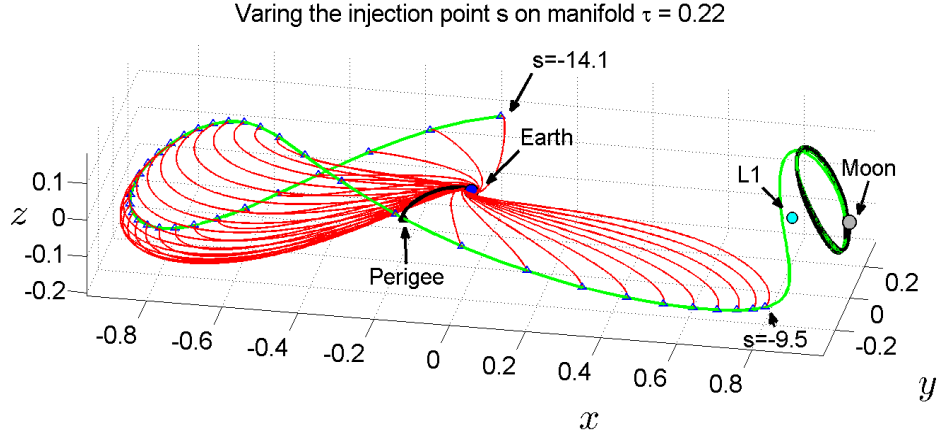


Figure 8. Transfer to different manifold injection point s on stable manifold associated with $\tau = 0.22$. The black thick arc is the perigee transfer.

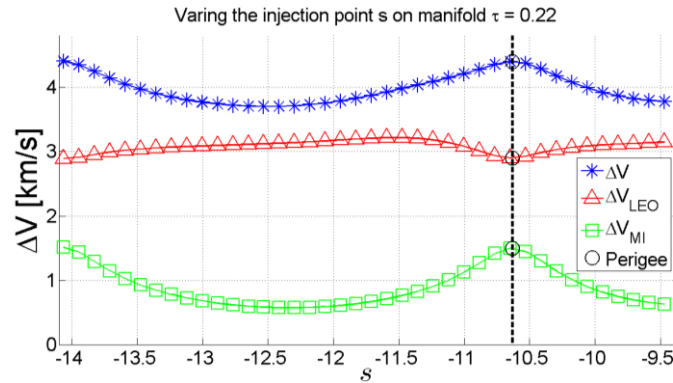


Figure 9. Velocity cost curves of different manifold injection point s on stable manifold associated with $\tau = 0.22$.

From this point of view the optimal MI point transfer to different OI points τ on ME-Halo can be constructed. The procedure is only different from the perigee transfer at the choice of the MI point, which is determined through an optimization process here. Then two tangent maneuvers are established for the bridge segment to glue the parking LEO and the optimal MI point in similar way. But there will be many local extremes since the manifold will rotate the Earth for many circles. In this paper, the MI point s is limited between the first epoch when $x < 0.8$ and the second epoch when $x = 0$, the same as that of Fig. 8, during which the manifold passes at least one perigee and one apogee. The velocity cost of the external optimal transfers are illustrated in Fig. 10. The ΔV ranges from 3.388 km/s to 3.934 km/s, which is much less than that of perigee transfers. There is clear periodicity for the ΔV_{MI} curve but not for other two curves. The discontinuity is as well caused by the restriction on the MI point.

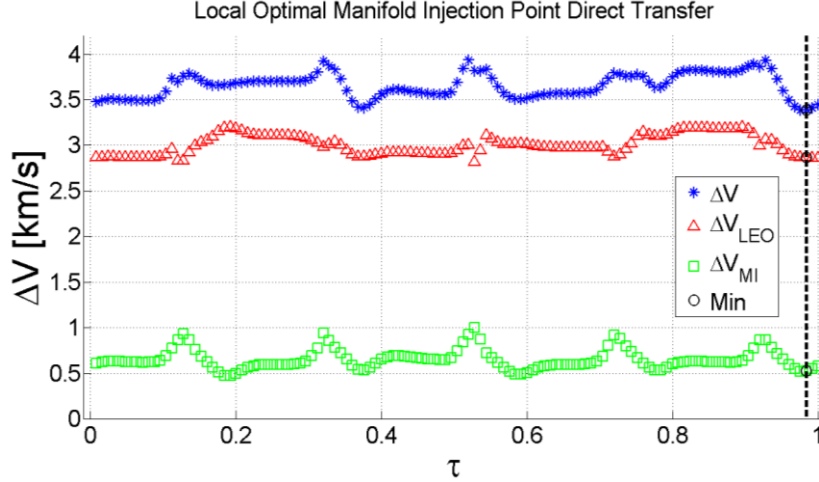


Figure 10. Velocity cost curves of different orbit injection points τ by optimal external direct transfer.

4. Redundant Stable Direction

As has been discussed, the lunar ME-Halo orbit can possess two pairs of real eigenvalues and hence two stable manifold directions for each point on the orbit. In this section a preliminary study of this redundant stable direction is expressed through the L_1 Periapsis ME-Halo orbits with $M5N2$. The monodromy matrix Ψ has two eigenvalues smaller than one, $\lambda_1 = 4.07 \times 10^{-5}$ and $\lambda_2 = 0.978$. Although eigenvalues are invariant along the ME-Halo orbit, the characteristic directions varies. The OI point $\tau = 0$ is chosen and fixed for the demonstration. At this point, the smaller λ_1 gives the main stable direction v_1^s and the smaller one gives the redundant direction v_2^s . Their positive directions are set to be consistent with the synodic frame. It is important to understand that they span a hyperplane tangent to the orbit at τ in phase space, and they form a skew-coordinate frame with an angle $\gamma \approx 40.2^\circ$ as illustrated in Fig. 11. Four quadrants are given by $\beta \in (0, \gamma)$, $(\gamma, 180^\circ)$, $(180^\circ, \gamma + 180^\circ)$ and $(\gamma + 180^\circ, 0)$. Only the first and the third quadrant are determined to give internal manifolds and external manifolds respectively because they have same positive directions. In other two quadrants the tendency changes at a certain angle. In Fig. 12 manifolds generated by from different quadrants are demonstrated. The green arc represents the main manifold given by v_1^s and the magenta arc represents the redundant manifold given by v_2^s . It is clear that in the first and third quadrant manifolds given by v_1^s and v_2^s are boundaries of all possible manifolds. However, in the second and fourth quadrant the main direction manifold (green) is not the boundary anymore but some other manifolds can reach further. The Floquet theory cannot explain it since the main stable manifold occupies the smallest eigenvalue and hence should reach the furthest during backward integral.

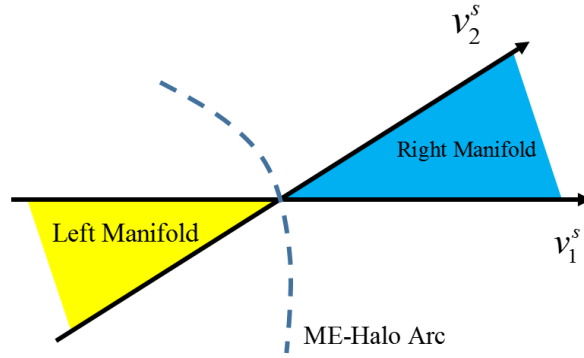


Figure 11. Hyperplane spanned by two stable manifold directions of the fixed point on the ME-halo orbit. They form a skew-coordinate frame. Only the first and third quadrant can be determined to generate manifolds towards the right and left side of the orbit.

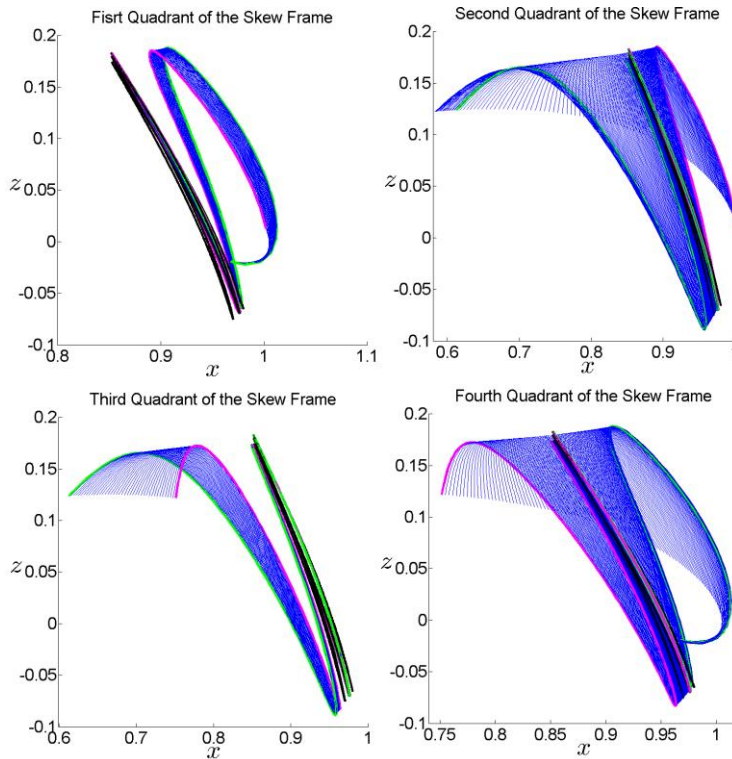


Figure 12 Four quadrants of the two-dimensional manifolds associated with orbit injection point $\tau = 0$. The black arc is the ME-Halo orbit. The green arc represents the main stable direction. The magenta arc represents the second stable direction. They are boundaries in the first and the second quadrant but not in the third and the fourth.

This redundant direction can great benefit the direct transfer design. The ME-Halo in ERTBP has a strict constrain on the epoch and the primary phase because of its non-autonomy, so the transfer trajectory is also strictly constrained to each time epoch. But this redundant dimension frees this limitation to some extent since at any epoch a small bias can locate the spacecraft on another nearby transfer trajectory. However, the optimization space is increased by one dimension as well, thus computational time greatly increased and even worse more local minimums could arise. Moreover, from this point of view it can be more helpful in station-keeping strategy design

since the manifold of ME-Halo orbits is three-dimensional and intersections nearly always exist, which can be used to guide the spacecraft.

5. Conclusion

ME-Halo orbits are strict periodic orbits only exist in the non-autonomous ERTBP model. Its period are M times of a traditional circular halo orbit and it can possess two-dimensional stable manifold at each point, which makes it a promising nominal orbit in space mission design. In this paper the direct transfer to lunar ME-Halo orbit with two impulsive maneuvers is constructed and optimized. The transfer trajectory is constructed by backward integration along stable manifold to the manifold injection (MI) point and a bridge segment connecting the parking LEO and the MI point. The MI point is first set to be the perigee and then freed to be optimized. Results show that different orbit injection points give different ΔV and optimal transfers occur around the apogee of manifolds. At the end the redundant stable direction is studied and its possible applications are discussed. It provides more allowance on trajectory design and possibly a new station-keeping strategy. Practically the ME-Halo orbit may serve as a relatively stable nominal orbit for observation missions or a nature formation fly orbit utilizing its multi-circle property. Its properties are complex and further studies are required. As a conclusion, the ME-Halo orbit is of potential practicing value and it can be reached by direct transfer with two impulsive maneuver.

6. References

- [1] Meyer, K. R., Hall, G. R. and Offin, D., *Introduction to Hamiltonian Dynamical Systems and the N-Body Problem*, Springer New York, New York, NY, 2009.
- [2] Szebehely, V. G., *Theory of Orbits - The Restricted Problem of Three Bodies*, Academic Press, New York and London, 1967.
- [3] Farquhar, R. W. and Kamel, A. A., "Quasi-periodic orbits about the translunar libration point," *Celestial Mechanics*, Vol. 7, No. 4, pp. 458–473, 1973.
- [4] Richardson, D. L., "Analytic construction of periodic orbits about the collinear points," *Celestial Mechanics*, Vol. 22, No. 3, pp. 241–253, 1980.
- [5] Howell, K. C. and Pernicka, H. J., "Numerical determination of Lissajous trajectories in the restricted three-body problem," *Celestial Mechanics and Dynamical Astronomy*, Vol. 41, pp. 107–124, 1987.
- [6] Belbruno, E. A., Gidea, M. and Topputo, F., "Geometry of Weak Stability Boundaries," *Qualitative Theory of Dynamical Systems*, 2012.
- [7] Lo, M. W., Marsden, J. E. and Ross, S. D., *Dynamical System, the Three-Body Problem, And Space Mission Design*, 2006.

- [8] Koon, W. S., Lo, M. W., Marsden, J. E. and Ross, S. D., “Shoot the moon,” *Orbit An International Journal On Orbital Disorders And Facial Reconstructive Surgery*, pp. 1–14, 2000.
- [9] Gómez, G., Koon, W. S., Lo, M. W., Marsden, J. E., Masdemont, J. J. and Ross, S. D., “Connecting orbits and invariant manifolds in the spatial restricted three-body problem,” *Nonlinearity*, Vol. 17, No. 5, pp. 1571–1606, 2004.
- [10] Parker, J. S. and Anderson, R. L., *Low-Energy Lunar Trajectory Design*, 2013.
- [11] Russell, R. P., “Survey of Spacecraft Trajectory Design in Strongly Perturbed Environments,” *Journal of Guidance, Control, and Dynamics*, Vol. 35, No. 3, pp. 705–720, 2012.
- [12] Moulton, F. R., *Periodic Orbits*, Washington Carnegie Institution of Washington, Washington, 1920.
- [13] Broucke, R. A., “Stability of periodic orbits in the elliptic, restricted three-body problem,” *AIAA Journal*, Vol. 7, No. 6, pp. 1003–1009, 1969.
- [14] Sarris, E., “Families of symmetric-periodic orbits in the elliptic three-dimensional restricted three-body problem,” *Astrophysics and Space Science*, Vol. 162, No. 1, pp. 107–122, 1989.
- [15] Hou, X. Y. and Liu, L., “On motions around the collinear libration points in the elliptic restricted three-body problem,” *Monthly Notices of the Royal Astronomical Society*, Vol. 415, No. 4, pp. 3552–3560, 2011.
- [16] Campagnola, S., “New techniques in astrodynamics for moon systems exploration,” University Of Southern California, 2010.
- [17] Qi, R., Xu, S., Zhang, Y. and Wang, Y., “Earth-to-Moon Low Energy Transfer Using Time-dependent Invariant Manifolds,” *AIAA/AAS Astrodynamics Specialist Conference*, Reston, Virginia, pp.1–11, 2012.
- [18] Qi, R., Xu, S. and Xu, M., “Impulsive Control for Formation Flight About Libration Points,” *Journal of Guidance, Control, and Dynamics*, Vol. 35, No. 2, pp. 484–496, 2012.
- [19] Qi, Y., Xu, S. and Qi, R., “Study of the gravitational capture at mercury in the elliptic restricted three-body problem,” *Proceedings 24th International Symposium on Space Flight Dynamics – 24th ISSFD*, 2014.
- [20] Peng, H. and Xu, S., “Numerical stability study of multi-circle elliptic halo orbit in the elliptic restricted three-body problem,” *Proceedings 24th International Symposium on Space Flight Dynamics – 24th ISSFD*, Luarel, United State, pp.1–20, 2014.